Strain-Induced Interference Effects on the Resonance Raman Cross Section of Carbon Nanotubes

A. G. Souza Filho,[1,*] N. Kobayashi,[2] J. Jiang,[2] A. Grüneis,[2] R. Saito,[2] S. B. Cronin,[3] J. Mendes Filho,[1] Ge. G. Samsonidze,[4] G. Dresselhaus,[5] and M. S. Dresselhaus[4,6]

[1]*Departamento de Física, Universidade Federal do Ceará, Fortaleza-CE, 60455-760, Brazil*
[2]*Department of Physics, Tohoku University, and CREST, JST, Sendai 980-8578, Japan*
[3]*Department of Electrical Engineering, University of Southern California, Los Angeles, California 90089, USA*
[4]*Department of Electrical Engineering and Computer Science, Massachusetts Institute of Technology, Cambridge, Massachusetts 02139-4307, USA*
[5]*Francis Bitter Magnet Laboratory, Massachusetts Institute of Technology, Cambridge, Massachusetts 02139-4307, USA*
[6]*Department of Physics, Massachusetts Institute of Technology, Cambridge, Massachusetts 02139-4307, USA*

(Received 19 February 2005; published 17 November 2005)

In this Letter, we report the effects of strain on the electronic properties of single-wall carbon nanotubes. When we normalize the electronic transition energies to the corresponding values obtained for unstrained tubes, we obtain that, regardless of the tube diameter, all the data collapse onto universal curves following an $n - m =$ constant family pattern. In the case of metallic tubes, quantum interference effects on the Raman cross section are predicted for strained tubes when the energies of the lower and the upper components have nearly the same values. Experimental evidence for the strain-induced Raman cross section changes is observed in single nanotube spectroscopy.

DOI: 10.1103/PhysRevLett.95.217403 PACS numbers: 78.67.Ch, 78.30.Na

Single-wall carbon nanotubes (SWNTs) are unique prototype materials for modeling one-dimensional systems. The recent development of scanning probe techniques has allowed clever experiments to be carried out on individual nanotubes. These experiments have opened up many new opportunities for learning new physical concepts, not only about nanotubes themselves but also about low-dimensional systems in general [1]. In particular, both experimental [2–6] and theoretical [7–10] reports have pointed out the strong sensitivity of the electronic properties of SWNTs to strain. Understanding the effects of this variable on SWNT properties is a key point for integrating SWNTs with other systems where the nanotubes will always be perturbed to some extent by their environment. Yang *et al.* [7,11] have derived analytical expressions and have also performed numerical simulations for explaining the chirality dependence of their electronic transitions. Recently, Capaz *et al.* [8] calculated the changes in the band gap of semiconducting SWNTs under uniaxial strain and found an $n - m$ family pattern. The changes in the band gap E_{gap} of semiconducting SWNTs through mechanical strain have been experimentally verified by employing an atomic force microscope (AFM) tip to simultaneously vary the strain σ while applying a gate voltage to the SWNT [4]. The $dE_{\text{gap}}/d\sigma$ is positive (negative) if $p = 1$ ($p = -1$) in the $n - m = 3q + p$ equation, where q is an integer and the (n, m) pair defines the atomic structure of the SWNTs [12]. Recently, the hydrostatic pressure coefficients of interband transitions dE_{ii}/dP for SWNTs dispersed in sodium dodecyl sulfate (SDS) were measured by optical absorption and emission experiments [5]. Both dE_{11}/dP and dE_{22}/dP were found to be negative for all SWNTs observed in the experiment, with the absolute value changing for each (n, m) pair. The effects of pressure are more pronounced for E_{11} than for E_{22}, with the dE_{22}/dP values being smaller in magnitude than dE_{11}/dP. Up to now, most experimental studies on strained tubes were performed on semiconducting (S) tubes [2,5].

The observed band-gap photoluminescence (PL) from SDS wrapped SWNTs opened up new opportunities for accessing the E_{11}^{S} and E_{22}^{S} energy transition values by analyzing absorption and emission optical data [13]. The PL technique, however, can be applied only to semiconducting tubes. For metallic SWNTs, the PL maps cannot be measured, and other techniques, such as resonance Raman spectroscopy (RRS), are needed. Nowadays, RRS studies on single tubes are well established, and joint experiments with scanning probes are becoming a reality [2]. By combining RRS with a tunable laser experiment, one can probe details of the electronic band structure of metallic SWNTs. Such studies should reveal new physical phenomena, since each subband for metallic (M) tubes has two components due to the trigonal warping effect [14]. The separation of the peaks depending on their (n, m) values, and an understanding of how their (n, m) affect their Raman cross sections, is fundamental for characterizing strained SWNTs either as isolated tubes [2] or in ensembles like in a hydrostatic pressure experiment [5] or for SWNTs dispersed into composites [3].

In this Letter, we report the effects of radial and uniaxial strain on the electronic properties of SWNTs. The electronic transitions E_{ii} between van Hove singularities in the valence and conduction bands are affected by strain σ. We find that the $E_{ii}(\sigma)$ (strained tubes)/$E_{ii}(0)$ (unstrained

tubes) ratio R_S follows $n - m =$ constant patterns and the R_S for all the SWNTs collapse to the same curve, regardless of tube diameter. This effect is observed for both metallic and semiconducting SWNTs. For metallic tubes, the lower and the upper components of E_{ii} resulting from the trigonal warping effect are affected differently, and, for low chiral angles, they cross for some particular strain value. Near (at) the crossing point, the resonant Raman spectra profile exhibits a maximum (minimum) value due to a quantum interference in the Raman cross section. In this work, evidence of this Raman cross section interference effect was observed in Raman experiments carried out on isolated SWNTs.

We have calculated the strain ratio R_S for 84 different SWNTs, including 42 semiconducting and 42 metallic SWNTs. The diameter range was $0.70\ \text{nm} \leq d_t \leq 1.35\ \text{nm}$, covering the d_t range of most current synthesis methods. The starting point in our calculations is the (n, m) structure after geometrical optimization [15,16], and the resulting electronic band structure is calculated by using an extended tight-binding model (ETB) that successfully accounts for the family patterns observed in the PL emission data [17]. It should be pointed out that the effect of many body corrections on the ETB results is to shift the transition energies [18], and this correction has been considered in our results presented here. By using the optimized structural data, we then considered strain-induced changes in either the tube diameter (radial strain) and/or the tube length (uniaxial strain). The applied changes varied from -2% up to $+2\%$ of the optimized diameter and tube length.

Our calculated results show that the electronic transition energies E_{ii}^{S} are highly affected by both radial and uniaxial strain σ, and the sign and magnitude of the slope $dE_{ii}^{\mathrm{S}}/d\sigma$ depend on the (n, m) values and the index i of the subbands for each SWNT. Qualitatively, our results agree with those reported previously by Yang *et al.* [7,11]. The discrepancies come from differences in the tight-binding parameters used in the two calculations. Our set of parameters nicely fits the E_{ii} values observed in the absorption and emission optical data [16]. The family pattern for all tubes with the same $n - m$ value is seen in the collapse of the normalized $E_{ii}(\sigma)/E_{ii}(0)$ data and is seen for both the radial and the uniaxial strain for the E_{11}^{S} transition. The data for E_{22}^{S} exhibit the same family behavior, but the slopes are smaller in magnitude and they have an opposite sign with respect to the results for E_{11}^{S}. It should be noted that, within the same i subband, the slope for the uniaxial strain is opposite in sign to that of the radial strain, as can be seen by comparing Figs. 1(a) and 1(b). The effect of a 1% uniaxial strain is enough to change the transition energy by 20% for some $n - m$ universal curve families, which should result in a 50 meV change in E_{ii}^{S}. This value is larger than the resonance window for Raman scattering for an isolated SWNT [19] and also larger than the linewidth of PL peaks observed in SDS wrapped tubes,

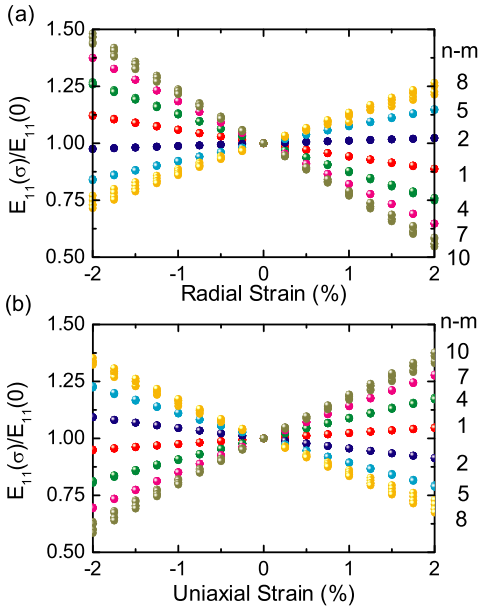

FIG. 1 (color online). The $E_{11}^{S}(\sigma)/E_{11}^{S}(0)$ ratio for different strain levels σ for semiconducting SWNTs. (a) and (b) display this ratio for a radial and uniaxial strain, respectively, for several $n - m$ families. The $n - m$ family indices are listed on the right side of each panel.

and this value should affect both the Raman and the PL spectra [13].

The collapse of the data for the $n - m$ families into universal curves can be understood as follows. If the trigonal warping effect is neglected, the transition energies scale with d_t^{-1}. When we normalize the strained $E_{ii}(\sigma)$ values by the unstrained value $E_{ii}(0)$, we are pulling out the d_t dependence of the electronic transitions. The data collapse into curves following an $n - m$ family pattern is due to chirality effects arising from the trigonal warping effect that spreads out the E_{ii} values at constant d_t in the Kataura's plot [14].

The effects of strain on the properties of metallic SWNTs were also studied. For metallic SWNTs, it is necessary to consider the trigonal warping effect and its consequence on the electronic properties. Depending on the tube chirality, this effect causes a splitting of each van Hove singularity for metallic nanotubes into lower (E_{ii}^{L}) and higher (E_{ii}^{H}) energy components. These transitions are defined for zero strain. The magnitude of this splitting varies from zero for armchair nanotubes (n, n) to a maximum splitting for metallic zigzag nanotubes $(3n, 0)$, where n is an integer [14]. The $E_{ii}^{\mathrm{L}}(\sigma)/E_{ii}^{\mathrm{L}}(0)$ normalized strain ratio for metallic tubes also follows an $n - m$ family pattern, as shown in Fig. 2 for the lower component of E_{11}^{M}. The electronic density of states (DOS) for the $(11, 5)$ SWNT under varying amounts of uniaxial strain is shown in Fig. 3(a). The strain induces a small gap in the DOS (see dotted circle) that progressively increases for both positive and negative strain. Therefore, the strain induces an observable metallic-semiconducting transition when $k_B T$ is

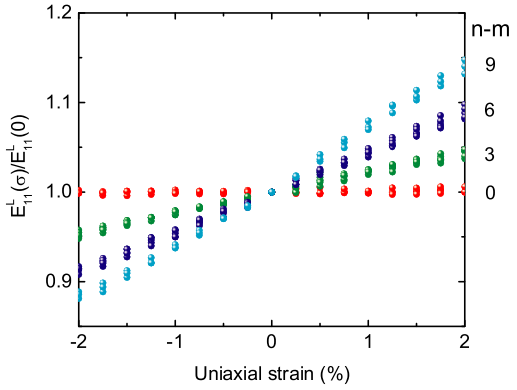

FIG. 2 (color online). The $E_{11}^{L}(\sigma)/E_{11}^{L}(0)$ ratio for different uniaxial strain levels for metallic SWNTs. Data are for the lower component of E_{11}^{M}.

lower than the energy of the minigap. Under uniaxial strain, the lower $[E_{11}^{L} = E(c_1^{L}) - E(v_1^{L})]$ and higher $[E_{11}^{H} = E(c_1^{H}) - E(v_1^{H})]$ energy components of E_{11}^{M} for the (11, 5) tube cross at about +1% strain [see Fig. 3(b)] because one of the energies decreases and the other increases as the strain increases. $E(v)$ $[E(c)]$ denotes the energy of the top (bottom) of the valence (conduction) band. Strain affects the valence and conduction bands differently, as we can see for $E(v_1^{L})$ and $E(v_1^{H})$ that cross at a strain of 1%. The same observation is valid for $E(c_1^{L})$ and $E(c_1^{H})$. However, the crossing point occurs at different strain values because, in the ETB model, the valence and conducting bands are not symmetrical to one another, with the valence bands being more flat and closer to each other than the conduction bands. The trend described above is similar for all zigzag and chiral metallic tubes. This crossing phenomenon has strong effects on the RRS cross section for the radial breathing mode (RBM), as we discuss next in connection with experiments.

Since strain significantly modifies the SWNT electronic structure, drastic changes in the resonant Raman profile of strained individual SWNTs are expected. Measurement of

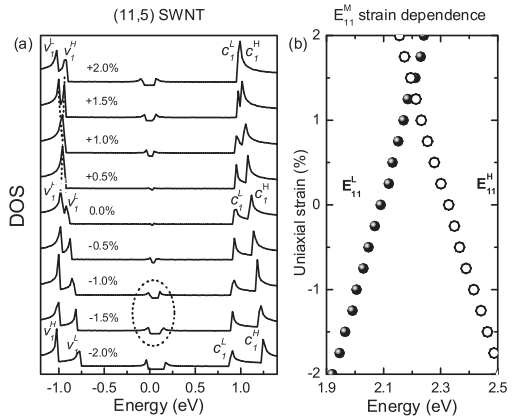

FIG. 3. (a) The calculated electronic DOS and (b) electronic transition energies $E_{11}^{L,H}$ for the (11, 5) SWNT under different uniaxial strain conditions.

the RRS profile of one individual SWNT is possible by combining a tunable laser system [19] with AFM strained nanotubes [2]. The resonant scattering profile for the Stokes process can be predicted from [20–22]

$$I_S(E_L) = C(n_{\mathrm{ph}} + 1)\left(\frac{E_a}{E_e}\right)^2\left(\frac{T_L}{N_c}\right)\left|\sum_{\mu=0}^{N-1} I^{\mu}(E_L)\right|^2, \quad (1)$$

where C is a constant, independent of the (n, m) tube, E_a and E_e denote the absorption and the emission photon energies, respectively, n_{ph} is the phonon thermal factor given by $n_{\mathrm{ph}} = (e^{-E_{\mathrm{ph}}/k_B T} - 1)^{-1}$, N_c and T_L denote the number of cutting lines and the 1D unit vector length of the SWNT, respectively, while γ is the inverse of the lifetime for the excited states. $I^{\mu}(E_L)$ is the contribution to $I_S(E_L)$, the Raman intensity of the μth band energy in Eq. (1):

$$I^{\mu}(E_L) = \int \frac{M^{\mathrm{op}} M_{\mathrm{ep}} M^{\mathrm{op}} dk}{[E_L - E_{\mu}(k) - i\gamma][E_L - E_{\mu}(k) - E_{\mathrm{ph}} - i\gamma]}. \quad (2)$$

The optical matrix element M^{op} for the electron-photon coupling and M_{ep} for the electron-phonon coupling are calculated using previously reported methods [21,23]. In Fig. 4(a), we show a 2D plot for the RBM RRS intensity profile for (15, 3) SWNTs under different strain conditions. The darkest (red color) areas indicate high intensity. Here it is seen that the resonance with E_{11}^{H} has a much lower intensity than that of E_{11}^{L}. This is due to the smaller magnitude of the matrix element along $K - \Gamma$ than that in the $K - M$ direction [21]. This theoretical prediction is in agreement with experimental observations, where only one peak has been observed in the RRS data for metallic SWNTs dispersed in a surfactant [24].

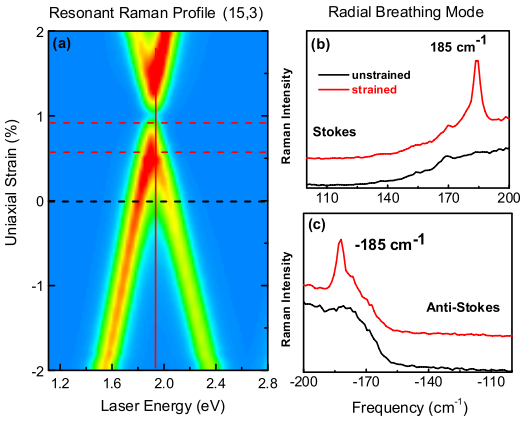

FIG. 4 (color online). (a) 2D plot for the calculated resonance Raman profile for a (15, 3) SWNT under different uniaxial strain conditions. The red (blue) areas indicate high (low) intensity. The vertical line stands for $E_{\mathrm{laser}} = 1.956$ eV used for measuring the spectra shown in panels (b) and (c). (b) and (c) stand for the Stokes and anti-Stokes RBM Raman spectra, respectively, measured under different strain conditions and performed on an isolated SWNT tentatively assigned as (15, 3).

By observing the RRS profile in Fig. 4(a), two remarkable effects are emphasized. First, we have a negative effect (intensity suppression) due to a quantum interference effect when $E_{11}^{H} \approx E_{11}^{L}$. Second, there is a positive effect (intensity enhancement) just before and after the crossing point (red areas in Fig. 4 online). Thus, by using a tunable laser system, it should be possible to follow the whole process of the quantum interference effect as both effects are turned on and off. To observe the quantum interference effect predicted in this Letter, we should select SWNTs with a low chiral angle (near zigzag tubes) such as the (15, 3) SWNT that is measured in the experiments [Figs. 4(b) and 4(c)]. The reason for needing tubes with a low chiral angle is that the M_{ep} matrix element can then have large values for both E_{11}^{L} and E_{11}^{H} and, thus, the quantum interference effect is strong.

We should point out here that our model did not consider the exciton-phonon coupling effect in the calculation of the Raman cross section. It is known that many body corrections (taking into account electron-electron repulsion and electron-hole attraction) have a net effect on the order of 0.1 eV [25–28]. These corrections have been empirically introduced for shifting the energies obtained through the extended tight-binding model [18]. The modifications of the many body corrections by strain is a perturbation, and, thus, the correction due to strain to the calculated energies should be much less than 0.1 eV, especially for SWNTs with $d_t > 1.0$ nm. Then our predictions should be valid within the approximations we used.

Finally, we discuss an experimental result that supports our predictions. RRS experiments were performed on nearly uniaxially strained isolated metallic tubes where the strain was induced by pushing the SWNT with an atomic force microscope tip. The experiment was performed on an isolated metallic SWNT lying on a SiO_2 substrate using the same setup as described in Ref. [2]. The Stokes and anti-Stokes spectra for a SWNT with an RBM frequency at 185 cm^{-1} are shown in Figs. 4(b) and 4(c). The lower (upper) trace is for an unstrained (strained) SWNT. The experimental strain value determination is not precise and has an error bar of 0.2%. The Raman signal shown in Figs. 4(b) and 4(c) is for a tube with strain around 0.8%. The strain uncertainty is represented in Fig. 4(a) by the region between the two red horizontal dashed lines. This tube is tentatively assigned to (15, 3), using the methods available in the literature and established for isolated tubes lying on a Si/SiO_2 substrate [29]. When the tube was unstrained, we could not observe the RBM, but, when the tube was exposed to strain, the intensity was dramatically enhanced. This drastic change in the Raman intensity is consistent with the calculation where a strain of about 0.8% is predicted by the constructive interference effect, thus enhancing the Raman signal [see red areas in Fig. 4(a) online].

In summary, we have calculated the effects of strain on the electronic properties of single-wall carbon nanotubes. The band structure has been calculated by using an extended tight-binding model with geometrical optimization [15,16]. The electronic transitions energies E_{ii} are highly affected by the strain, and they exhibit universal curves for the same $n - m =$ constant family, regardless of the tube diameter. A quantum interference effect has been predicted for the radial breathing mode spectra for metallic tubes. These strain-induced phenomena occur when the two components E_{11}^{L} and E_{11}^{H} have nearly the same value. The Raman experiment performed on an isolated strained metallic SWNT provides evidence for our modeling predictions.

A. G. S. F. acknowledges the JST for supporting his visit to Tohoku University, CNP_q (Grant No. 307417/2004-2) and UFC for partial support. R. S. acknowledges MEXT Grant No. 16076201. The MIT authors acknowledge support under NSF Grant No. DMR-04-05538.

*Electronic address: agsf@fisica.ufc.br

[1] M. S. Dresselhaus and H. Dai, MRS Bull. **29**, 237 (2004).
[2] S. B. Cronin *et al.*, Phys. Rev. Lett. **93**, 167401 (2004).
[3] M. Lucas and R. J. Young, Phys. Rev. B **69**, 085405 (2004).
[4] E. D. Minot *et al.*, Phys. Rev. Lett. **90**, 156401 (2003).
[5] J. Wu *et al.*, Phys. Rev. Lett. **93**, 017404 (2004).
[6] M. D. Frogley *et al.*, Phys. Rev. B **65**, 113413 (2002).
[7] L. Yang and J. Han, Phys. Rev. Lett. **85**, 154 (2000).
[8] R. B. Capaz *et al.*, Phys. Status Solidi B **241**, 3352 (2004).
[9] Y. Zhao *et al.*, Chem. Phys. Lett. **387**, 149 (2004).
[10] H. Jiang *et al.*, Phys. Rev. B **70**, 125404 (2004).
[11] L. Yang *et al.*, Phys. Rev. B **60**, 13 874 (1999).
[12] R. Saito *et al.*, *Physical Properties of Carbon Nanotubes* (Imperial College Press, London, 1998).
[13] M. J. O'Connell *et al.*, Science **297**, 593 (2002).
[14] R. Saito *et al.*, Phys. Rev. B **61**, 2981 (2000).
[15] V. N. Popov, New J. Phys. **6**, 17 (2004).
[16] G. G. Samsonidze *et al.*, Appl. Phys. Lett. **85**, 5703 (2004).
[17] P. G. Collins *et al.*, Science **292**, 706 (2001).
[18] A. Jorio *et al.*, Phys. Rev. B **71**, 075401 (2005).
[19] A. Jorio *et al.*, Phys. Rev. B **65**, 155412 (2002).
[20] R. M. Martin and L. M. Falicov, *Light Scattering in Solids* (Springer-Verlag, Berlin, 1975), p. 80.
[21] J. Jiang *et al.*, Phys. Rev. B **71**, 205420 (2005).
[22] G. Bussi *et al.*, Phys. Rev. B **71**, 041404 (2005).
[23] J. Jiang *et al.*, Carbon **42**, 3169 (2004).
[24] C. Fantini *et al.*, Phys. Rev. Lett. **93**, 147406 (2004).
[25] C. L. Kane and E. J. Mele, Phys. Rev. Lett. **90**, 207401 (2003).
[26] V. Perebeinos *et al.*, Phys. Rev. Lett. **92**, 257402 (2004).
[27] V. Perebeinos *et al.*, Phys. Rev. Lett. **94**, 027402 (2005).
[28] C. D. Spataru *et al.*, Phys. Rev. Lett. **92**, 077402 (2004).
[29] M. S. Dresselhaus *et al.*, Carbon **40**, 2043 (2002).